

# BEC-BCS Crossover of a Trapped Two-Component Fermi Gas with Unequal Masses

J. von Stecher,<sup>1</sup> Chris H. Greene,<sup>1</sup> and D. Blume<sup>1,2</sup>

<sup>1</sup>*JILA and Department of Physics, University of Colorado, Boulder, CO 80309-0440*

<sup>2</sup>*Department of Physics and Astronomy, Washington State University, Pullman, Washington 99164-2814*

(Dated: January 3, 2022)

We determine the energetically lowest lying states in the BEC-BCS crossover regime of  $s$ -wave interacting two-component Fermi gases under harmonic confinement by solving the many-body Schrödinger equation using two distinct approaches. Essentially exact basis set expansion techniques are applied to determine the energy spectrum of systems with  $N = 4$  fermions. Fixed-node diffusion Monte Carlo methods are applied to systems with up to  $N = 20$  fermions, and a discussion of different guiding functions used in the Monte Carlo approach to impose the proper symmetry of the fermionic system is presented. The energies are calculated as a function of the  $s$ -wave scattering length  $a_s$  for  $N = 2 - 20$  fermions and different mass ratios  $\kappa$  of the two species. On the BEC and BCS sides, our energies agree with analytically-determined first-order correction terms. We extract the scattering length and the effective range of the dimer-dimer system up to  $\kappa = 20$ . Our energies for the strongly-interacting trapped system in the unitarity regime show no shell structure, and are well described by a simple expression, whose functional form can be derived using the local density approximation, with one or two parameters. The universal parameter  $\xi$  for the trapped system for various  $\kappa$  is determined, and comparisons with results for the homogeneous system are presented.

PACS numbers:

## I. INTRODUCTION

Advances in trapping and cooling have spawned the experimental realization of ultracold externally-confined two-component Fermi gases with controllable interaction strengths. Using these impurity-free systems, the crossover from a weakly-attractive atomic Fermi gas through a strongly-interacting unitarity regime to a weakly-repulsive molecular Bose gas has been investigated [1, 2, 3, 4]. Our increased understanding of these systems relates to the study of neutron matter and potentially that of high- $T_c$  superconductors, in addition to the field of ultracold atomic gases. All of these systems are controlled by similar pairing mechanisms, although at much different densities.

To date, experimental studies of the BEC-BCS crossover with ultracold atomic gases have been restricted to fermions in different hyperfine substates. In this case, the “spin-up” and “spin-down” fermions have equal masses and experience equal trapping frequencies. Currently, the simultaneous trapping and cooling of different atomic fermionic species is being pursued in a number of laboratories. This motivates us to investigate how the BEC-BCS crossover physics changes with the mass ratio  $\kappa$  of the two atomic species. Our goal is to develop a microscopic understanding of these intricate many-body systems. To this end, we consider trapped systems with varying number of particles  $N$ , and relate them to the homogeneous systems through the local density approximation (LDA). This illuminates the transition from the few-body to the many-body physics of an ultracold Fermi gas.

For a given short-range two-body potential, the stationary Schrödinger equation for a trapped two-component Fermi gas has a rich eigenspectrum, which in

some cases includes deeply- and/or weakly-bound cluster states as well as “ground” and highly-excited gas-like states. In general, the eigenstates of two-component Fermi gases with short-range interactions can be separated into two classes: universal states that do not (or only weakly) depend on the details of the two-body potential [5], and non-universal states that depend notably on the details of the two-body potential. The eigenstates of the four-fermion system with equal masses, e.g., fall into the former class, provided the range of the two-body potential is sufficiently small; in this case, the properties of the system are to a very good approximation determined by a single parameter, the  $s$ -wave scattering length  $a_s$ . For large mass ratios, however, non-universal bound trimer states exist [6, 7, 8]. A description of these states requires a three-body parameter, which depends on the short-range physics. In some cases, non-universal bound clusters consisting of four or more fermions may exist. In this work, we do not analyze the properties of such non-universal states but instead study the properties of states that depend at most weakly on the short-range physics. In particular, we determine the BEC-BCS energy crossover curve, which is defined in Sec. III A, by solving the stationary Schrödinger equation for various mass ratios  $\kappa$ . An analysis of the stability of two-component Fermi systems with large mass ratios, including molecular Bose gases created from two-component Fermi gases, is beyond the scope of this paper.

Consider the stationary solutions of the four-particle system as a function of  $\kappa$  in the BEC-BCS crossover. The Schrödinger equation is solved in two distinct approaches: a basis set expansion technique that utilizes correlated Gaussians (CG) and a fixed-node diffusion Monte Carlo (FN-DMC) approach. The dimer-dimer scattering length  $a_{dd}$  and the dimer-dimer effective range

$r_{dd}$  emerge as a function of  $\kappa$ . A surprisingly large  $r_{dd}$  is found, which is likely to be an important input parameter in the BEC many-body theory. Furthermore, a detailed comparison of the results throughout the entire crossover regime permits a non-trivial test of the nodal surface employed in the FN-DMC approach, and it conveys information about the symmetry of the many-body wave function. Extension of our FN-DMC calculations to larger numbers of particles also probes the validity range of the analytically-determined limiting behaviors in the deep BCS and BEC regimes. In the strongly-interacting unitarity regime, the LDA relates the trapped system properties to those of the homogeneous system. Finally, our FN-DMC energies should allow for a stringent test of numerically less involved approaches such as density functional treatments [9].

Section II introduces the Hamiltonian of the trapped Fermi system, and the numerical approaches applied to solve the corresponding stationary many-body Schrödinger equation. Section III presents our results for the energetics and the interpretation of the results of weakly- and strongly-interacting Fermi systems with up to 20 atoms. Finally, Sec. IV concludes.

## II. HAMILTONIAN AND NUMERICAL APPROACH

### A. Hamiltonian

For  $N$  harmonically-trapped Fermi atoms divided equally into two species, the Hamiltonian is given by

$$H = \sum_{i=1}^{N/2} \left( \frac{-\hbar^2}{2m_1} \nabla_i^2 + \frac{1}{2} m_1 \omega_1^2 \vec{r}_i^2 \right) + \sum_{i'=1}^{N/2} \left( \frac{-\hbar^2}{2m_2} \nabla_{i'}^2 + \frac{1}{2} m_2 \omega_2^2 \vec{r}_{i'}^2 \right) + \sum_{i=1}^{N/2} \sum_{i'=1}^{N/2} V(r_{ii'}). \quad (1)$$

Here, unprimed indices label mass  $m_1$  and primed indices mass  $m_2$  fermions, and  $N$  is assumed to be even. The mass ratio  $\kappa$  is defined by  $m_1/m_2$  and throughout we take  $m_1 \geq m_2$ . In Eq. (1),  $\omega_1$  and  $\omega_2$  denote angular trapping frequencies, and  $\vec{r}_i$  the position vector of the  $i$ th fermion.

We adopt two purely attractive short-range model potentials for the interaction between unlike fermions: a Gaussian interaction potential  $V(r)$ ,  $V(r) = -V_0 \exp(-r^2/(2R_0^2))$ , and a square well interaction potential  $V(r)$ ,  $V(r) = -V_0$  for  $r < R_0$  and 0 otherwise. For a fixed range  $R_0$  of the two-body potential  $V(r)$ , the depth  $V_0$ ,  $V_0 \geq 0$ , is adjusted until the  $s$ -wave scattering length  $a_s$  assumes the desired value. For negative (or positive)  $a_s$ ,  $V_0$  and  $R_0$  are chosen so the potential supports no (or one) two-body  $s$ -wave bound state. Throughout this paper, we treat the like atoms as non-interacting. This is justified because the interactions between like atoms are only non-negligible very close to a  $p$ -wave Feshbach resonance. All experiments to date have studied

the BEC-BCS crossover using magnetic field strengths for which the  $p$ -wave interactions are non-resonant.

The Hamiltonian given by Eq. (1) is characterized by four different length scales: the range  $R_0$  of the interaction potential, the  $s$ -wave scattering length  $a_s$ , and the two oscillator lengths  $a_{ho}^{(j)} = \sqrt{\hbar/(m_j \omega_j)}$ ,  $j = 1$  and  $2$ . Throughout, we are interested in the regime where  $R_0$  is much smaller than the oscillator lengths  $a_{ho}^{(j)}$ , or equivalently, where the system is dilute with respect to  $R_0$ , i.e.,  $n(0)R_0^3 \ll 1$ , where  $n(0)$  denotes the peak density. In this regime, the properties of the universal states are expected to be independent of the details of the two-body potential. For a given  $a_s$ , we numerically test whether a state is universal by calculating its energy for various  $R_0$ . The condition  $R_0 \ll a_{ho}^{(j)}$  implies that the numerical approaches chosen for solving the many-body Schrödinger equation have to be able to govern the physics occurring at at least two different length scales. As we illustrate below, the CG and FN-DMC approaches are able to do so.

### B. Correlated Gaussian approach

The correlated Gaussian method[10, 11] is a powerful tool to study few-body systems. Recently, the CG approach has been applied to the four-fermion system with equal masses [12]. Here, we analyze the properties of this system from a somewhat different point of view and additionally consider the unequal mass system. As in the previous work, we treat equal trapping frequencies, i.e.,  $\omega_1 = \omega_2$ , so that the center-of-mass motion separates. To further reduce the dimensionality of the problem, we restrict ourselves to states with vanishing total angular momentum  $L$  and positive parity  $P$ . We expand the  $L^P = 0^+$  states in terms of correlated Gaussian basis functions  $\Phi_{\vec{d}}$ , which depend on the six interparticle distances and the center of mass vector,

$$\psi(\vec{r}_1, \vec{r}_2, \vec{r}'_1, \vec{r}'_2) = \sum_{\{\vec{d}\}} C_{\vec{d}} \Phi_{\vec{d}}. \quad (2)$$

Here, the  $C_{\vec{d}}$  denote expansion coefficients. Each basis function  $\Phi_{\vec{d}}$  is written as a product of the ground state center-of-mass wavefunction and a symmetrized product of Gaussian functions for each interparticle distance vector [12]. The widths of these Gaussians can be different for each interparticle distance, giving us six parameters for each basis function. These parameters are in Eq. (2) collectively denoted by  $\vec{d}$ . The simple functional form of the wave function  $\psi$ , Eq. (2), allows the analytical determination of all matrix elements if the two-body interaction potential is taken to be a Gaussian (see Sec. II A).

The parameter vector  $\vec{d}$  that characterizes each basis function  $\Phi_{\vec{d}}$  are selected semi-randomly. Typically, the components of  $\vec{d}$  vary from a fraction of the range  $R_0$  to a few times the interparticle distance in the noninteracting limit. The basis functions can be roughly separated

into three types. The first type has all the components of  $\vec{d}$  of the order of the trap lengths and is suitable to describe gas-like states. The second type has one or two small  $\vec{d}$  components while the others take values of the order of the trap lengths; these basis functions carry a large weight when  $\psi$  describes states that consist—to a good approximation—of two bound dimers or a dimer and two free atoms. The third type has more than two small  $\vec{d}$  components, and is suitable to describe comparatively tightly-bound three- and four-body states. In general, all three types of basis functions are needed to accurately describe the entire  $L^P = 0^+$  spectrum of the four-fermion system. For equal masses, however, we find that the third type carries negligible weight, owing to the absence of molecular three- or four-body states. As the mass ratio increases, more basis functions of the third type need to be included. We carefully check the convergence of the energies by varying the total number of basis functions used, and by varying the basis functions included in the expansion. We find that of the order of  $10^4$  basis functions suffice to accurately describe the eigenfunctions of interest.

The basis functions introduced above are not linearly independent. To eliminate the linear dependence in our basis set, we diagonalize the overlap matrix and eliminate the basis functions with the lowest eigenvalues up to a certain cutoff. The remaining basis functions are then used to construct a new orthogonal basis set. Finally, the eigenspectrum is obtained by diagonalizing the corresponding Hamiltonian matrix.

### C. Fixed-node diffusion Monte Carlo approach

To treat up to  $N = 20$  fermions, solutions of the Schrödinger equation are determined by the FN-DMC method [13, 14]. In this method, the proper fermionic antisymmetry is imposed through the use of a so-called guiding function  $\psi_T$ , which depends on the coordinates of all particles. To within statistical uncertainties, the FN-DMC algorithm provides an upper bound to the exact ground state energy, i.e., to the lowest-lying state with the same symmetry as  $\psi_T$ . Note that all our FN-DMC calculations are performed for the square well interaction potential. While there is no technical problem in extending the FN-DMC calculations to the Gaussian interaction potential, the guiding functions  $\psi_T$  are most readily determined and evaluated for the square well potential.

Two different guiding functions  $\psi_T$  considered in this work are:

$$\psi_{T1} = \prod_{i=1}^{N/2} \Phi(\vec{r}_i/a_{ho}^{(1)}) \times \prod_{i'=1}^{N/2} \Phi(\vec{r}_{i'}/a_{ho}^{(2)}) \times \mathcal{A}(f(r_{11'}), \dots, f(r_{N/2, N/2'})) \quad (3)$$

TABLE I: FN-DMC energies  $E$  in units of  $\hbar\bar{\omega}$  as a function of  $N$ ,  $N = 2 - 20$ , for the two-component Fermi system with  $a_{ho}^{(1)} = a_{ho}^{(2)}$  at unitarity for  $\kappa = 1$  and 8. Statistical uncertainties of the energies are reported in round brackets. Note that no nodal approximation needs to be made for  $N = 2$ .

$N$	$E(N)/(\hbar\bar{\omega})$ ( $\kappa = 1$ )	$E(N)/(\hbar\bar{\omega})$ ( $\kappa = 8$ )
2	2.00202(3)	1.726(7)
4	5.069(9)	4.48(1)
6	8.67(3)	7.82(3)
8	12.57(3)	11.39(4)
10	16.79(4)	15.28(6)
12	21.26(5)	19.45(6)
14	25.90(5)	23.81(6)
16	30.92(6)	28.46(7)
18	36.00(7)	33.42(8)
20	41.35(8)	38.11(9)

and

$$\psi_{T2} = \Psi_{NI}(\vec{r}_1, \dots, \vec{r}_{N/2'}) \times \prod_{i,i'}^{N/2} \bar{f}(r_{ii'}), \quad (4)$$

Here  $\Phi$  denotes the ground state harmonic oscillator orbital,  $\mathcal{A}$  is the antisymmetrizer, and  $\Psi_{NI}$  denotes the wave function of  $N$  trapped non-interacting fermions. Following Ref. [15], the pair function  $f$  is constructed from the free-space zero-energy scattering and the free-space bound state solution of the two-body square-well interaction potential for negative and positive  $s$ -wave scattering length  $a_s$ , respectively. In Eq. (4),  $\bar{f}$  coincides with  $f$  for small  $r$  and is matched smoothly to a non-zero constant at larger  $r$ . This matching to a non-zero constant ensures that the product over all pair functions  $\bar{f}$  is always non-zero. Thus, the nodal structure of  $\psi_{T2}$  coincides with that of the non-interacting Fermi gas. In contrast, the nodal surface of  $\psi_{T1}$  is constructed by antisymmetrizing a product of pair functions [15].

To assess the accuracy of our MC code, we determine the energy of the two-body system with  $\omega_1 = \omega_2$  and  $m_1 = m_2$  semi-analytically. We separate off the center-of-mass motion, and write the eigenfunctions of the Schrödinger equation for the relative coordinate in terms of hypergeometric functions. The resulting eigenequation results in an energy of  $E = 2.00200\hbar\bar{\omega}$ . Since the two-body wave function is nodeless, the DMC energy for  $N = 2$  (see Table I) is expected to be exact. Indeed, the DMC energy agrees to within the statistical uncertainty with the energy determined semi-analytically. A detailed comparison of the FN-DMC and CG energies for the four-fermion system, which allows the quality of the nodal surface employed in the FN-DMC calculations to be assessed, is presented in Sec. III B.

In the non-interacting case, i.e., for  $a_s = 0$ , the guiding function  $\psi_{T2}$  with  $\bar{f}(r) = 1$  coincides with the exact eigen function. For weakly-attractive Fermi systems, the

attractive nature of the two-body potential introduces correlations but does, to a good approximation, leave the nodal surface unchanged. Indeed, we find that the variational energy for  $\psi_{T1}$  in this regime is nearly indistinguishable from the FN-DMC energies, indicating that the Jastrow product over all pair functions accounts properly for the two-body correlations of the system and that three- and higher-order correlations are negligible.

For small positive  $a_s$ , on the other hand, comparatively strongly-bound two-body dimers exist and the system is expected to form a molecular Bose gas of dimers. Such a system is not even qualitatively described correctly by the guiding function  $\psi_{T1}$ , which assumes that every spin-up fermion is “simultaneously” correlated with every spin-down fermion [16]. The guiding function  $\psi_{T2}$ , instead, is much better suited to describe a Fermi gas that behaves as a weakly-interacting molecular Bose gas.  $\psi_{T2}$  correlates the first spin-up fermion with the first spin-down fermion, the second spin-up fermion with the second spin-down fermion, and so on, and then antisymmetrizes this “paired state”. The guiding function  $\psi_{T2}$  is expected to accurately describe the system when the size of the dimer pairs becomes small compared to the oscillator lengths.

Finally, in the strongly-interacting regime, i.e., for  $|a_s| \rightarrow \infty$ , it is not *a priori* clear which of the two guiding functions provides a better description of the system. Section III discusses this in more detail, and also comments on additional aspects of the choice of the guiding functions related to the existence of non-universal trimer states.

### III. RESULTS

#### A. Energy crossover curve: Definition and general considerations

Throughout this work, we are interested in describing the crossover from a weakly-repulsive to a weakly-attractive trapped two-component Fermi system with  $N$  particles. This BEC-BCS crossover can be characterized by the normalized energy crossover curve  $\Lambda_N^{(\kappa)}$ ,

$$\Lambda_N^{(\kappa)} = \frac{E(N) - NE(2)/2}{\lambda \hbar \bar{\omega}}, \quad (5)$$

which depends on  $a_s$ ,  $\kappa$  and  $N$ . In Eq. (5),  $E(N)$  denotes the energy of the  $N$ -fermion system,  $\bar{\omega} = (\omega_1 + \omega_2)/2$  is the average frequency and  $\lambda$  is defined through the energy  $E_{NI}$  of  $N$  non-interacting fermions,

$$E_{NI} = (\lambda + 3N/2)\hbar\bar{\omega}. \quad (6)$$

The values of  $\lambda$  for the first few closed-shell systems are listed in the second column of Table II.  $\Lambda_N^{(\kappa)}$  equals one on the deep BCS side (small  $|a_s|$  and  $a_s < 0$ ), and zero on the deep BEC side (small  $a_s$  and  $a_s > 0$ ). Since the energy  $E(2)$  of  $N/2$  trapped dimer pairs is subtracted

from the total energy  $E(N)$  of the system, the energy crossover curve  $\Lambda_N^{(\kappa)}$ , Eq. (5), is expected to be independent of the details of the two-body potential if the range  $R_0$  is much smaller than the average interparticle spacing. The energy crossover curve defined here for the trapped system is the analog of the BEC-BCS crossover curve of the homogeneous system (see, e.g., Refs. [17, 18, 19] for pioneering work based on the mean-field BCS equations, and Figs. 1 and 2 of Ref. [15] for a determination of the crossover curve for the homogeneous system by the FN-DMC method).

As indicated above,  $\Lambda_N^{(\kappa)}$  depends on the scattering length  $a_s$ , the number of particles  $N$ , the ratio between the two masses, and the ratio between the two frequencies. Thus, an exhaustive study of the whole parameter space of trapped two-component Fermi systems by first principle methods is impossible. This paper considers two different scenarios: i) the trapping frequencies are set to coincide, i.e.,  $\omega_1 = \omega_2$ , while  $\kappa$ ,  $N$  and  $a_s$  are varied (see Secs. III B and III C), and ii) the oscillator lengths are set to coincide, i.e.,  $a_{ho}^{(1)} = a_{ho}^{(2)}$ , and  $1/|a_s|$  is set to 0, while  $N$  and  $\kappa$  are varied (see Sec. III D).

Our motivation for considering scenario i) is as follows. In the deep BEC regime, the fermionic system is expected to form a molecular Bose gas whose behaviors are to a good approximation determined by the dimer-dimer scattering length  $a_{dd}$ . The dimer-dimer scattering length can be extracted quite readily for different  $\kappa$  from our four-body energies, provided the center-of-mass motion decouples (see Sec. III B). For unequal frequencies, the center-of-mass motion does not decouple and the extraction of the dimer-dimer scattering length would be more involved. Section III C extends the study of the four-fermion system with equal frequencies to systems with more particles to illustrate that the behaviors of the larger systems in the deep BEC regime are also governed to a good approximation by the dimer-dimer scattering length. While this has been shown to be the case previously for the homogeneous system with equal masses [15], our calculations illustrate that—as might be expected—the many-body physics of unequal mass systems in the deep BEC regime is also to a good approximation governed by a single few-body parameter, the dimer-dimer scattering length. In the more strongly-interacting regime, our equal frequency calculations for  $\kappa > 1$  provide insights into the behaviors of systems whose densities are not fully overlapping. Thus, mass-imbalanced Fermi system may behave in certain respects similar to population-imbalanced Fermi systems.

Our primary motivation for considering scenario ii) is to connect the behaviors of the trapped system with those of the homogeneous system using the LDA. The energy of the homogeneous system at unitarity is related to the energy of the non-interacting system by a universal parameter  $\xi$ . By calculating the energies of the trapped system at unitarity for equal frequencies and equal masses, we quantify how well the LDA describes small trapped sys-

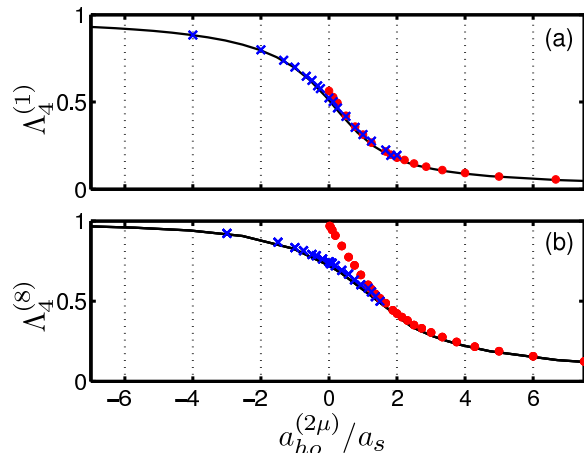


FIG. 1: (Color online) Energy crossover curve  $\Lambda_4^{(\kappa)}$  for  $\omega_1 = \omega_2$  as a function of  $a_{ho}^{(2\mu)}/a_s$  for (a)  $\kappa = 1$  and (b)  $\kappa = 8$ . Solid lines are calculated by the CG approach, and circles and crosses by the FN-DMC method using  $\psi_{T1}$  and  $\psi_{T2}$ , respectively.

tems. Unpublished results for the homogeneous system with equal spin-up and spin-down densities but unequal masses indicate that the universal parameter  $\xi$  depends weakly on the mass ratio  $\kappa$  [20]. These unequal mass results for the homogeneous system cannot be straightforwardly connected to those of the trapped system since the densities of the two trapped species do not necessarily fully overlap. In the non-interacting limit, the densities of the two species coincide when the trapping lengths are equal, i.e.,  $a_{ho}^{(1)} = a_{ho}^{(2)}$ . At unitarity, we find that unequal mass systems with  $a_{ho}^{(1)} = a_{ho}^{(2)}$  have a small, though non-negligible, density mismatch. Despite this small density mismatch, we apply the LDA  $a_{ho}^{(1)} = a_{ho}^{(2)}$  and relate the universal parameter of the homogeneous system to the energetics of the trapped system.

### B. Energy crossover curve for $N = 4$

This subsection presents our results for the energy crossover curve for four trapped fermions calculated by the CG and FN-DMC approaches for equal frequencies, i.e.,  $\omega_1 = \omega_2 = \bar{\omega}$ , and varying mass ratio  $\kappa$ .

Figure 1 shows the energy crossover curve  $\Lambda_4^{(\kappa)}$  for four fermions as a function of  $a_{ho}^{(2\mu)}/a_s$  calculated by the CG and FN-DMC approaches for (a)  $\kappa = 1$  and (b)  $\kappa = 8$ . Here, the oscillator length  $a_{ho}^{(2\mu)}$  is defined in terms of the reduced mass  $\mu = m_1 m_2 / (m_1 + m_2)$ , i.e.,  $a_{ho}^{(2\mu)} = \sqrt{\hbar / (2\mu\bar{\omega})}$ . The solid lines in Fig. 1 are obtained using  $E(4)$  calculated by the CG approach, while circles and crosses are obtained using  $E(4)$  calculated by the FN-DMC approach using  $\psi_{T1}$  and  $\psi_{T2}$ , respectively. The ranges  $R_0$  of the two-body potentials used in Fig. 1 are much smaller than the oscillator lengths, i.e.,

$R_0 \approx 0.01 a_{ho}^{(2\mu)}$ . From our CG energies for different  $R_0$ , we estimate that the  $\Lambda_N^{(\kappa)}$  shown in Fig. 1 deviate by at most 1% from the corresponding curves for zero-range interactions. For  $m_1 = m_2$ , e.g., the energy at unitarity calculated by the CG approach for the Gaussian interaction potential is  $E = 5.027\hbar\bar{\omega}$  for  $R_0 = 0.01 a_{ho}^{(2\mu)}$  and  $E = 5.099\hbar\bar{\omega}$  for  $R_0 = 0.05 a_{ho}^{(2\mu)}$  [5]. For comparison, the FN-DMC energy for the square well potential with  $R_0 = 0.01 a_{ho}^{(2\mu)}$  is  $E = 5.069(9)$  (see Table I), which is in good agreement with the energies calculated by the CG approach.

As expected, the energy crossover curve connects the limiting values of one on the BCS side and zero on the BEC side smoothly. Importantly, the lowest FN-DMC energies and the CG energies agree well, which implies that the functional forms of  $\psi_{T1}$  and  $\psi_{T2}$  are adequate. For equal masses [panel (a)], the FN-DMC energies at unitarity calculated using the two different  $\psi_T$  agree approximately. For unequal masses [panel (b)], in contrast, the nodal surface of  $\psi_{T2}$  leads to a lower energy at unitarity than that of  $\psi_{T1}$ , and the crossing point between the energies calculated using  $\psi_{T1}$  and  $\psi_{T2}$  moves to the BEC side. This can be understood by realizing that the densities of the heavy and light particles do not overlap fully, leading to a reduced pairing.

The CG approach in our current implementation (see Sec. II B) allows for the determination of the complete  $L^P = 0^+$  energy spectrum. If we use short-range Gaussian two-body potentials that support no two-body  $s$ -wave bound state for negative  $a_s$  and one two-body  $s$ -wave bound state for positive  $a_s$ , the four-body energy that enters the calculation of the energy crossover curves shown in Fig. 1 is the true ground state of the system, i.e., no energetically lower-lying bound trimer or tetramer states with  $L^P = 0^+$  symmetry exist. For larger mass ratios, bound trimer states exist. The mass ratio at which these non-universal trimer states appear depends on the range  $R_0$  of the two-body potential employed. In the regime where three-body bound states exist, the four-body spectrum calculated by the CG approach contains also universal states which are separated by approximately  $2\hbar\bar{\omega}$  and which can be best described as two weakly-interacting composite bosons. For fixed  $a_s$ ,  $a_s > 0$ , the energy of these “dimer-dimer states” changes smoothly as a function of  $\kappa$  even in the regime where bound trimer states appear. In the following, we use these dimer-dimer states to extract the dimer-dimer scattering length as a function of  $\kappa$  up to  $\kappa = 20$ .

When  $a_s$  is small, the four fermions form two bosonic molecules of mass  $M$ , where  $M = m_1 + m_2$ , which interact through an effective molecule-molecule potential [8]. To model this effective dimer-dimer potential (the exact functional form is unknown), we introduce a regularized zero-range potential  $V(r)$  [21],  $V(r) = g\delta(\vec{r})(\partial/\partial r)r$ , whose scattering strength  $g$  is parameterized by the scattering length  $a_{dd}$  and the effective range  $r_{dd}$  of the dimer-

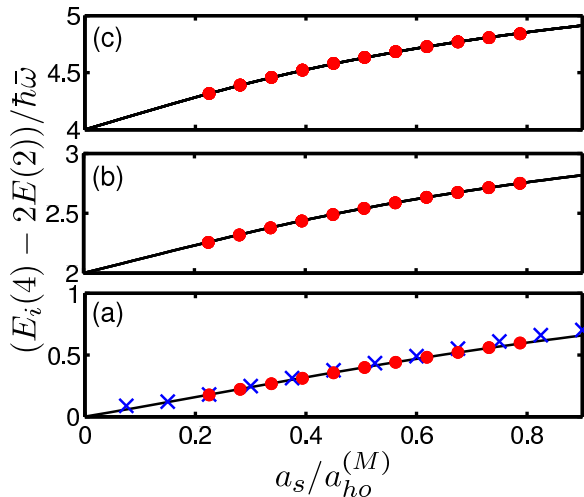


FIG. 2: (Color online) Four-body energies of the three energetically lowest-lying dimer-dimer states as a function of  $a_s/a_{ho}^{(M)}$  for  $\kappa = 8$ . Panel (a) shows the energetically lowest lying energy level ( $i = 0$ ), panel (b) the energetically second lowest ( $i = 1$ ) and panel (c) the energetically third lowest state ( $i = 2$ ). Circles and crosses show our CG and FN-DMC results, respectively. Solid lines show the zero-range model results.

dimer system, i.e.,

$$g = \frac{4\pi\hbar^2 a_{dd}}{M} \left[ 1 - \frac{ME_{tb}r_{dd}a_{dd}}{2\hbar^2} \right]^{-1}. \quad (7)$$

Here,  $E_{tb}$  denotes the relative energy of the two-boson system, i.e., the total energy with the center-of-mass contribution subtracted. It has been shown previously [22, 23] that the inclusion of the energy dependence of the scattering length notably extends the validity regime of the zero-range pseudopotential when applied to describe the scattering of two atoms under external confinement. By comparing the “dimer-dimer energy levels” of the four-fermion system with the energies of two mass  $M$  bosons in a trap interacting through this energy-dependent zero-range potential [22, 23, 24], we determine  $a_{dd}$  and  $r_{dd}$ .

To illustrate this procedure, circles in Figs. 2(a) through (c) show the three energetically lowest-lying dimer-dimer energy levels, referred to as  $E_i(4)$  with  $i = 0$  through 2, with the center-of-mass energy and the dimer-binding energy subtracted for  $\kappa = 8$  obtained by the CG approach as a function of  $a_s$ . Solid lines show the energy levels obtained by fitting these four-body energies by the two-boson energies obtained using the energy-dependent zero-range pseudopotential ( $a_{dd}$  and  $r_{dd}$  are treated as fitting parameters). We find that inclusion of the effective range  $r_{dd}$  extends the validity regime over which the four-fermion system can be described by the two-boson model and additionally allows for a more reliable determination of  $a_{dd}$ . Figure 2 illustrates that the two-boson spectrum reproduces the dimer-dimer states of the four-

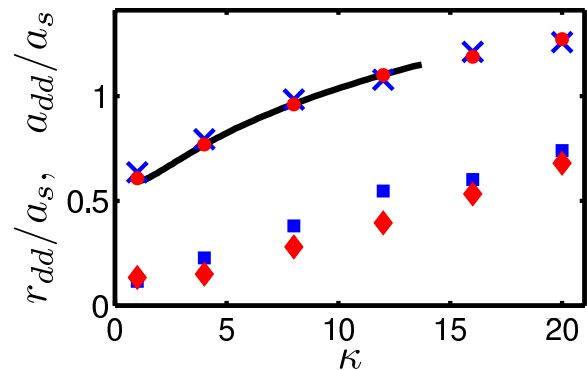


FIG. 3: (Color online) Circles and crosses show  $a_{dd}/a_s$  as a function of  $\kappa$  extracted from the four-fermion CG and FN-DMC energies, respectively. For comparison, a solid line shows the results from Fig. 3 of Ref. [8]. Diamonds and squares show  $r_{dd}/a_s$  extracted from the four-fermion CG and FN-DMC energies, respectively.

fermion spectrum well over a fairly large range of atom-atom scattering lengths  $a_s$ . For comparison, crosses in Fig. 2(a) show the corresponding FN-DMC energies for the energetically lowest-lying dimer-dimer state. We did not attempt to construct a guiding function that would allow for the determination of excited dimer-dimer states. We find that the FN-DMC energies are slightly larger than the CG energies and that the deviation increases with increasing  $a_s$ . Presumably, this can be attributed to the functional form of the nodal surface used in the FN-DMC calculations, which should be best in the very deep BEC regime. The increasing deviation between the FN-DMC and CG energies with increasing  $a_s$  explains why the effective range predicted by the analysis of the FN-DMC energies is somewhat larger than that predicted by the analysis of the CG approach (see discussion of Fig. 3 below).

Circles and crosses in Fig. 3 show the resulting dimer-dimer scattering lengths  $a_{dd}$  extracted from the energies calculated by the CG and the FN-DMC approach, respectively, as a function of  $\kappa$ . For all mass ratios considered in Fig. 3, we include up to three dimer-dimer energy levels in our analysis of the CG results, and only the lowest dimer-dimer level in our analysis of the FN-DMC results. Our dimer-dimer scattering lengths agree well with those calculated by Petrov *et al.* within a zero-range framework [8] (solid line in Fig. 3). The calculations by Petrov *et al.*, performed for the free and not the trapped four-fermion system, terminate at  $\kappa \approx 13.6$ , beyond which a three-body parameter is needed to solve the four-body equations within the applied framework. Our calculations show the existence of deeply-bound “plunging” states, which consist of a trimer plus a free atom. This signals a qualitative change of the energy spectrum, in agreement with Petrov *et al.* [8]. At the same time, our calculations for finite-range potentials predict that  $a_{dd}$  continues to increase smoothly when the mass ratio

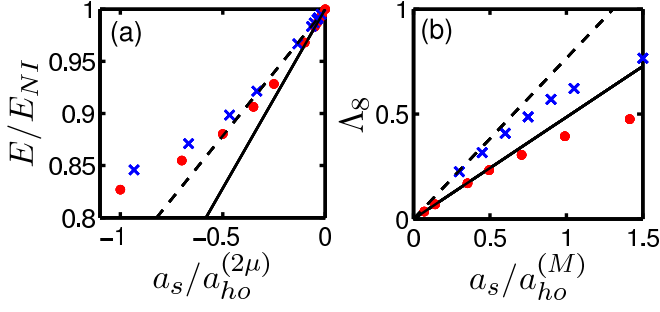


FIG. 4: (Color online) Energies for  $N = 8$  and small  $|a_s|$ . (a)  $E(8)/E_{NI}$  as a function of  $a_s/a_{ho}^{(2\mu)}$  for  $\omega_1 = \omega_2 = \bar{\omega}$  for  $\kappa = 1$  (circles and solid line) and  $\kappa = 8$  (crosses and dashed line). Symbols are calculated by the FN-DMC method using  $\psi_{T2}$ , and lines using the first order correction, Eq. (10). (b)  $\Lambda_8^{(\kappa)}$  as a function of  $a_s/a_{ho}^{(M)}$  for  $\omega_1 = \omega_2 = \bar{\omega}$  for  $\kappa = 1$  (circles and solid line) and  $\kappa = 8$  (crosses and dashed line). Symbols are calculated by the FN-DMC method using  $\psi_{T1}$ , and lines using the first order correction, Eq. (11).

$\kappa$  exceeds 13.6. This can possibly be explained by the fact that the presence of the external confining potential may “wash out” some of the features present in the free-space system. As already mentioned, the study of the stability of the four-fermion system, consisting of two dimers, with large mass ratios is beyond the scope of this work.

Diamonds and squares in Fig. 3 show the effective range  $r_{dd}$  extracted from our CG and FN-DMC energies, respectively. We estimate the uncertainty of  $r_{dd}$  obtained from the CG approach to be about 10%, and quite a bit larger for that extracted from the FN-DMC energies. Figure 3 shows that the ratio  $r_{dd}/a_{dd}$  increases from about 0.2 for  $\kappa = 1$  to about 0.5 for  $\kappa = 20$ . While earlier work already suggested that the dimer-dimer potential may be best characterized as a broad soft-core potential [8], implying a non-negligible value for the effective range  $r_{dd}$ , our work makes the first quantitative predictions for  $r_{dd}$  as a function of  $\kappa$ . The large value of  $r_{dd}$  suggests that effective range corrections may need to be considered in analyzing the physics of molecular Fermi gases.

### C. Weakly-interacting limits for $N > 4$

We now apply the FN-DMC method to larger systems with  $\omega_1 = \omega_2 = \bar{\omega}$ , focussing on the deep BCS and BEC regimes where  $|a_s|$  is small. Figure 4(a) shows the total energy  $E(N)$  for  $N = 8$  particles, divided by the energy  $E_{NI}$  of the non-interacting system, for  $\kappa = 1$  and 8 as a function of  $a_s/a_{ho}^{(2\mu)}$  for small  $|a_s|$ . The FN-DMC energies, calculated using  $\psi_{T2}$ , are shown by symbols (circles for  $\kappa = 1$  and crosses for  $\kappa = 8$ ).

For comparison, we calculate the energy of a weakly-attractive closed-shell Fermi system with equal frequencies ( $\bar{\omega} = \omega_1 = \omega_2$ ) in first order perturbation theory. We

TABLE II: Values of  $\lambda$  and  $C_N^\kappa$  for the four smallest closed-shell two-component Fermi systems with equal frequencies.

$N$	$\lambda$	$C_N^\kappa$
2	0	$\sqrt{\frac{2}{\pi}}$
8	6	$\sqrt{\frac{2}{\pi}} \frac{(4+23\kappa+4\kappa^2)}{(1+\kappa)^2}$
20	30	$\sqrt{\frac{2}{\pi}} \frac{5(20+50\kappa+249\kappa^2+50\kappa^3+20\kappa^4)}{4(1+\kappa)^4}$
40	90	$\sqrt{\frac{2}{\pi}} \frac{5(40+450\kappa+306\kappa^2+2795\kappa^3+306\kappa^4+450\kappa^5+40\kappa^6)}{4(1+\kappa)^6}$

assume that the unlike fermions are interacting through the Fermi pseudopotential  $V_s(\vec{r}, \vec{r}') = \frac{2\pi\hbar^2 a_s}{\mu} \delta(\vec{r} - \vec{r}')$  [25]. Applying perturbation theory to the non-interacting two-component Fermi gas with unequal masses but equal frequencies, the energy becomes  $E \approx E_{NI} + E_{int}^{(1)}$ , where the first order energy correction  $E_{int}^{(1)}$  for closed-shell systems can be written as

$$E_{int}^{(1)} = \frac{2\pi a_s \hbar^2}{\mu} \int \rho_{m_1}(\vec{r}) \rho_{m_2}(\vec{r}) d\vec{r}. \quad (8)$$

Here,  $\rho_{m_i}$  denotes the density of a single non-interacting mass  $m_i$  component ( $i = 1$  and 2). The integration in Eq. (8) can be performed analytically, resulting in a simple expression for the first-order energy correction,

$$E_{int}^{(1)} = \hbar\bar{\omega} C_N^\kappa \frac{a_s}{a_{ho}^{(2\mu)}}, \quad (9)$$

where  $C_N^\kappa$  denotes a constant that depends on  $N$  and  $\kappa$ . Altogether, we obtain

$$E \approx E_{NI} + \hbar\bar{\omega} C_N^\kappa \frac{a_s}{a_{ho}^{(2\mu)}}. \quad (10)$$

The values of  $C_N^\kappa$  for the first four closed-shell systems are summarized in the third column of Table II. For completeness, the second column summarizes the values of  $\lambda$  that determine the energy  $E_{NI}$  of the non-interacting system [see Eq. (6)].

The first order correction, Eq. (10), is shown by solid and dashed lines in Fig. 4(a) for  $\kappa = 1$  and 8, respectively; it describes the interacting system well for  $|a_s| \leq 0.25 a_{ho}^{(2\mu)}$ , or equivalently, for  $k_F^0 a_s \leq 0.6$ . Here,  $k_F^0$  denotes the wave vector at the trap center of a non-interacting system of  $N$  fermions with mass  $2\mu$  evaluated within the Thomas Fermi approximation,  $k_F^0 = \sqrt{2}(3N)^{1/6}/a_{ho}^{(2\mu)}$ . Additional corrections can be derived within a renormalized scattering length framework [26].

We now turn to the small  $a_s$  limit for  $N = 8$ . Circles ( $\kappa = 1$ ) and crosses ( $\kappa = 8$ ) in Fig. 4(b) show the energy crossover curve  $\Lambda_8^{(\kappa)}$  in the BEC regime for  $\bar{\omega} = \omega_1 = \omega_2$ , where  $E(8)$  is calculated by the FN-DMC method, as a function of  $a_s/a_{ho}^{(M)}$ , where  $a_{ho}^M = \sqrt{\hbar/(M\bar{\omega})}$ ; in the small  $a_s$  regime,  $a_{ho}^{(M)}$  is the relevant characteristic oscillator length. Treating the  $N$ -fermion system as a bosonic

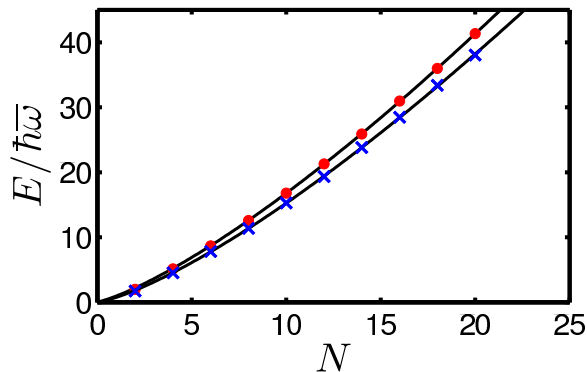


FIG. 5: (Color online) Circles and crosses show the FN-DMC energies  $E(N)$  in units of  $\hbar\bar{\omega}$  as a function of  $N$  at unitarity for  $\kappa = 1$  ( $\omega_1 = \omega_2$ ) and  $\kappa = 8$  ( $\omega_2 = \kappa\omega_1$ ), respectively. Solid lines show a fit of the FN-DMC energies to Eq. (13).

gas consisting of  $N/2$  mass  $M$  molecules and applying first order perturbation theory using a Fermi pseudopotential [25], the energy of the system with  $\bar{\omega} = \omega_1 = \omega_2$  reads

$$E \approx \frac{N}{2}E(2) + \hbar\bar{\omega} \frac{N(N-2)}{8} \sqrt{\frac{2}{\pi}} \frac{a_{dd}}{a_{ho}^{(M)}}. \quad (11)$$

Solid and dashed lines in Fig. 4(b) show  $\Lambda_s^{(\kappa)}$  for  $\kappa = 1$  and 8, respectively, calculated using Eq. (11). To plot the expansion, we use the dimer-dimer scattering length  $a_{dd}$  calculated by the CG approach. For both mass ratios, the agreement between the FN-DMC energies and the first order correction is good for  $a_s \leq 0.5a_{ho}^{(M)}$ . Figure 4(a) thus illustrates that the behavior of the Fermi system depends to a first approximation only on  $a_{dd}$  if  $a_s/a_{ho}^{(M)}$  is sufficiently small. Inclusion of effective range corrections may improve the agreement but is beyond the scope of this paper.

We checked that the behaviors discussed here for  $N = 8$  also hold for  $N = 20$  particles.

#### D. Energetics at unitarity

This section considers the strongly-interacting unitary regime, where the atom-atom scattering length is infinite. To ensure large overlap of the densities of the two species, we choose the trapping frequencies  $\omega_1$  and  $\omega_2$  so that  $a_{ho}^{(1)} = a_{ho}^{(2)}$  (see Sec. III A for a discussion). Circles and crosses in Fig. 5 show our FN-DMC energies  $E(N)$  at unitarity as a function of  $N$  for  $\kappa = 1$  and 8, respectively, while Table I lists the FN-DMC energies. In these calculations, the range  $R_0$  of the square well potential used to describe the interaction between unlike fermions is set to  $R_0 = 0.01a_{ho}^{(1)}$ . The energies for  $N = 4$  are calculated using  $\psi_{T2}$ ; usage of  $\psi_{T1}$  leads to slightly higher energies. As discussed already in Sec. III B, the four-body FN-DMC energy for equal masses agrees well with

the corresponding CG energy. The energies for  $N \geq 6$  are calculated using the guiding function  $\psi_{T1}$ . For example, usage of the guiding function  $\psi_{T2}$  gives an energy of  $12.64(2)\hbar\bar{\omega}$  for  $N = 8$  and  $\kappa = 1$  (which is, taken the statistical errorbars into account, just slightly higher than the energy calculated using  $\psi_{T1}$ ; see Table I), and an energy of  $43.2(1)\hbar\bar{\omega}$  for  $N = 20$  and  $\kappa = 1$  (which is notably higher than the energy calculated using  $\psi_{T1}$ ; see Table I).

For  $N > 8$ , our energies for equal masses and equal frequencies are consistently lower than those reported in Ref. [27]. For  $N = 20$ , e.g., we find  $E = 41.35(8)\hbar\bar{\omega}$  while Ref. [27] reports  $43.2(4)\hbar\bar{\omega}$ . We speculate that this discrepancy can be traced back to the nodal structure of the trial wave function employed, and possibly also to the larger range of the two-body potential employed in Ref. [27]. In agreement with Ref. [27], we find that the energies at unitarity show no shell structure.

Using the LDA, which should be valid for sufficiently large  $N$ , we relate the energy of the trapped Fermi system at unitarity to the universal parameter  $\xi_\kappa$  and  $E_{NI}$ , i.e.,

$$E(N) = \sqrt{\xi_\kappa} E_{NI}. \quad (12)$$

The parameter  $\xi_\kappa$  connects the energy per particle  $E_{hom}/N$  of the homogeneous system at unitarity and the energy per particle  $E_{FG}$  of the homogeneous non-interacting Fermi gas, i.e.,  $E_{hom}/N = \xi_\kappa E_{FG}$ . Here, we assumed that the functional dependence of  $E_{hom}/N$  on  $E_{FG}$  is the same for equal and unequal masses but that the universal parameter  $\xi$  depends on  $\kappa$ . Applying the extended Thomas-Fermi (ETF) model to  $E_{NI}$  [28], the energy of the trapped system at unitarity becomes

$$E(N) = \sqrt{\xi_\kappa} \hbar\bar{\omega} \frac{(3N)^{4/3}}{4} \left( 1 + c_\kappa \frac{(3N)^{-2/3}}{2} + \dots \right), \quad (13)$$

where  $c_\kappa = 1$ . The first term in Eq. (13) is often referred to as Thomas-Fermi (TF) approximation. We also attempted to fit our FN-DMC energies by functional forms different from Eq. (13), which included higher-order correction terms or terms with other powers of  $N$ ; however, none of the alternative functional forms considered improved the description of our numerical results. Fitting our equal mass energies to Eq. (13), treating  $\xi_\kappa$  as a parameter, we find  $\xi_1 = 0.465$ . Our  $\xi_1$  extracted from the trapped system is about 10% larger than that determined for the bulk system, i.e.,  $\xi_1 = 0.42(1)$  [15, 29], suggesting that one has to go to somewhat larger trapped systems to extrapolate the bulk  $\xi_1$  with high accuracy within the LDA. Although the  $\xi_1$  obtained from the fit to the energies of the trapped system is larger than the corresponding bulk value, it is worthwhile noting that the simple functional form given in Eq. (13) provides an excellent description of the energies of the trapped system.

For  $\kappa = 8$ , we find that our energies are best described if we treat  $\xi_8$  and  $c_8$  as fitting parameters, yielding  $\xi_8 = 0.417$  and  $c_8 = 0.27$ . The decrease of  $c_8$  compared to the value predicted by the ETF model is most likely related

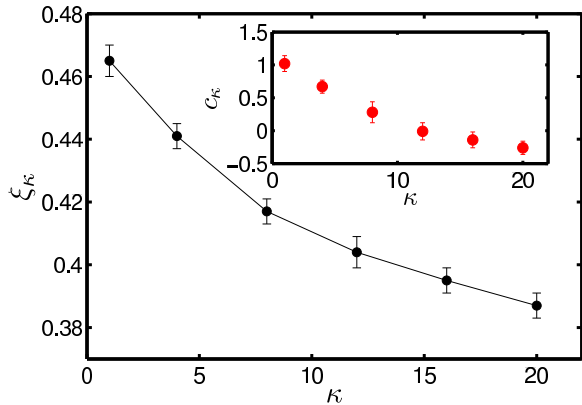


FIG. 6: (Color online)  $\xi_\kappa$  as a function of  $\kappa$ . Inset:  $c_\kappa$  as a function of  $\kappa$ . The errorbars indicate the uncertainty of the fitting parameters; this uncertainty does not include the statistical errors of the FN-DMC energies.

to the fact that the densities of the unequal mass species do, in contrast to the LDA treatment employed to derive Eq. (13), not fully overlap at unitarity. Our calculations suggest that the bulk value for  $\xi_\kappa$  is somewhat smaller for  $\kappa = 8$  than for  $\kappa = 1$ . To investigate this further, we additionally consider the energetics of systems with  $\kappa = 4, 12, 16$  and  $20$ . Figure 6 shows the resulting  $\xi_\kappa$  (main panel) and  $c_\kappa$  (inset) extracted from our energies for  $N = 2-20$  fermions as a function of  $\kappa$ . Both  $\xi_\kappa$  and  $c_\kappa$  vary smoothly, decrease with increasing  $\kappa$ , and seem to approach a constant for large  $\kappa$ . Furthermore,  $c_\kappa$  changes sign from positive to negative for  $\kappa \approx 10$ . We emphasize that Eq. (13) provides a rather good description of the energetics for all  $\kappa$  thus empirically motivating the non-constant coefficient  $c_\kappa$  of the correction term.

The fact that  $\xi_\kappa$  decreases with increasing  $\kappa$  is in agreement with recent FN-DMC calculations for the homogeneous system [20]. However, this decrease is more pronounced for the trapped system than for the homogeneous system. Standard BCS mean-field theory, in contrast, predicts that the parameter  $\xi$ , which determines many properties of dilute homogeneous two-component Fermi gases at unitarity [30], is independent of  $\kappa$  [31].

We now comment further on the choice of the guiding function used to obtain the energies for  $N = 2-20$  that enter into our determination of  $\xi_\kappa$  and  $c_\kappa$ . As mentioned earlier, trimer states with negative energy exist for  $\kappa = 16$  and  $20$ . If we use the guiding function  $\psi_{T2}$  to model these systems, many-body configurations that contain three particles in close proximity are being sampled, giving rise to negative energies at unitarity. However, if we use the guiding function  $\psi_{T1}$ , i.e., if we construct the nodal surface by pairing spin-up and spin-down particles, many-body configurations that contain tightly-bound trimer states are not being sampled. Thus, the guiding function  $\psi_{T1}$  allows for a numerically stable characterization of a state with positive energy that has the same symmetry as  $\psi_{T1}$ . We note that the decrease of  $\xi_\kappa$

with increasing  $\kappa$  is already present in the energies for the two-body system for which we can determine the energetics essentially exactly. This provides some evidence that the behaviors discussed in this section for unequal masses are not an artefact of our choice of guiding function.

The difference between the guiding functions  $\psi_{T1}$  and  $\psi_{T2}$  can also be understood from a different point of view. In the limit of vanishing confinement, the oscillator states used to construct  $\psi_T$  approach free-particle states. In this case, the nodal surface of the guiding function  $\psi_{T1}$  is compatible with a superfluid state, and the guiding function  $\psi_{T2}$  with a normal state [15, 29, 32, 33]. Using this analogy, our results suggest that even fairly small trapped Fermi systems are better described by a “superfluid wave function” than by a “normal wave function”. As  $N$  increases, the difference between the energies obtained for the superfluid and normal wave functions increases, presumably approaching the bulk values in the large  $N$  limit ( $E_{hom}/N = 0.42(1)E_{FG}$  [15, 29] for the superfluid state and  $E_{hom}/N = 0.54E_{FG}$  for the normal state [29, 32]).

#### IV. CONCLUSION

This paper characterizes the BEC-BCS crossover physics of trapped two-component Fermi gases with varying mass ratio. Our results are obtained by solving the stationary many-body Schrödinger equation for short-range model potential by two complementary approaches. For the four-particle system, an essentially exact basis set expansion type technique, a CG approach, is used to determine the complete  $L^P = 0^+$  spectrum. For up to  $N = 20$  particles, the FN-DMC approach is used to determine upper bounds for energy of the BEC-BCS crossover branch. Treating the four-body system is challenging, and interesting in its own right: The four-body system is the smallest non-trivial system exhibiting BEC-BCS crossover-like physics. Furthermore, the lessons learned from the four-body system aid the study of larger systems. Solving the Schrödinger equation for more than a few fermions by first principle methods is, despite the increasing available computer power, still a challenging task. In fact, it may be argued that Monte Carlo methods are the only methods suitable. Unfortunately however, assessing the accuracy of the assumptions going into Monte Carlo calculations, such as the nodal surface employed in the FN-DMC approach, remains a challenge. Our calculations, which use the CG and FN-DMC approaches in parallel, benchmark the strengths and limitations of the nodal surface employed in the FN-DMC calculations.

From our four-body calculations in the deep BEC regime, we determine the scattering length  $a_{dd}$  and effective range  $r_{dd}$  of the dimer-dimer system for two purely attractive short-range two-body potentials as a function of the mass ratio  $\kappa$ . For up to  $\kappa \approx 13.6$ , our dimer-dimer

scattering lengths  $a_{dd}$  agree well with the values calculated by Petrov *et al.* [8]. Our four-body calculations extend beyond this mass ratio  $\kappa$  and suggest that the energetically lowest-lying dimer-dimer state varies smoothly as a function of  $\kappa$ . We find that the energies of the dimer-dimer states for large  $\kappa$  depend, just as for small  $\kappa$ , at most weakly on the details of the two-body potential; we take this as numerical evidence that at least some properties of the dimer-dimer states are universal even if  $\kappa$  exceeds the value of 13.6. However, other properties of systems with large  $\kappa$  such as the system's stability, encapsulated in the three-body recombination rate, are presumably controlled by the details of the short-range potential. These non-universal properties should be investigated in the future. Also, future studies will have to investigate whether the comparatively large value of  $r_{dd}$  can be measured indirectly by, e.g., a careful analysis of the density profile in the BEC regime.

We also present calculations in the strongly-interacting

unitarity regime for different mass ratios. Our calculations for  $N = 2 - 20$  fermions show no shell structure. Application of the LDA to the trapped system implies that the universal parameter  $\kappa$  depends weakly on the mass ratio. Our energies at unitarity for various mass ratios may aid in developing and refining numerically less demanding treatments of two-component Fermi gases. Recently, e.g., Bulgac [9] proposed a density functional theory applicable to trapped equal-mass two-component Fermi gases at unitarity. Our results presented here provide much needed benchmarks for such theories. Our unequal mass studies present the first first principle treatment of such systems under confinement. Our analysis provides a first step towards a deeper understanding of these systems, but much room for further investigations, including the investigation of connections to mean-field treatments [31, 34, 35, 36, 37, 38, 39], remains.

We gratefully acknowledge discussions with S. Giorgini and S. Rittenhouse, and support by the NSF.

- 
- [1] C. A. Regal, C. Ticknor, J. L. Bohn, and D. S. Jin, *Nature* **424**, 47 (2003).
- [2] M. W. Zwierlein, C. A. Stan, C. H. Schunck, S. M. F. Raupach, S. Gupta, Z. Hadzibabic, and W. Ketterle, *Phys. Rev. Lett.* **91**, 250401 (2003).
- [3] K. E. Strecker, G. B. Partridge, and R. G. Hulet, *Phys. Rev. Lett.* **91**, 080406 (2003).
- [4] S. Jochim, M. Bartenstein, A. Altmeyer, G. Hendl, S. Riedl, C. Chin, J. Hecker Denschlag, and R. Grimm, *Science* **302**, 2101 (2003).
- [5] In the deep BEC regime, i.e., for small negative  $s$ -wave scattering length  $a_s$ , the energies of the BEC branches depend in general on the range  $R_0$  of the two-body potential. This dependence can, in principle, be eliminated by taking the limit  $R_0 \rightarrow 0$ . Throughout this work, we do not evaluate the  $R_0 \rightarrow 0$  limit for numerical reasons, and instead subtract the dimer binding energy [see Eq. (5)]. Consequently, we refer to states of the BEC branch as universal states if their energy, with the dimer binding energy subtracted, is independent of the range of the two-body potential.
- [6] V. N. Efimov, *Yad. Fiz.* **12**, 1080 (1970 [*Sov. J. Nucl. Phys.* **12**, 589 (1971)]).
- [7] V. N. Efimov, *Nucl. Phys. A* **210**, 157 (1973).
- [8] D. S. Petrov, C. Salomon, and G. V. Shlyapnikov, *J. Phys. B* **38**, S645 (2005).
- [9] A. Bulgac, *cond-mat/0703526* (2007).
- [10] K. Singer, *Proc. R. Soc. London, Ser. A* **258**, 412 (1960).
- [11] Y. Suzuki and K. Varga, *Stochastic Variational Approach to Quantum-Mechanical Few-Body Problems* (Springer-Verlag, Berlin, 1998).
- [12] J. von Stecher and C. H. Greene, *cond-mat/0701044* (2007).
- [13] P. J. Reynolds, D. M. Ceperley, B. J. Alder, and W. A. Lester, Jr., *J. Chem. Phys.* **77**, 5593 (1982).
- [14] B. L. Hammond, W. A. Lester, Jr., and P. J. Reynolds, *Monte Carlo Methods in Ab Initio Quantum Chemistry* (World Scientific, Singapore, 1994).
- [15] G. E. Astrakharchik, J. Boronat, J. D. Casulleras, and S. Giorgini, *Phys. Rev. Lett.* **93**, 200404 (2004).
- [16] The terms spin-up and spin-down are used figuratively. For equal masses, these terms refer to two atoms of the same isotope trapped in two different internal (hyperfine) states. For unequal masses, these terms refer to two different fermionic atoms, each trapped in a suitable internal (hyperfine) state.
- [17] A. J. Leggett, *Modern Trends in the Theory of Condensed Matter*, ed. by A. Pekalski and R. Przystawa (Springer Verlag, Berlin, 1980).
- [18] P. Nozières and S. Schmitt-Rink, *J. Low Temp. Phys.* **95**, 195 (1985).
- [19] J. R. Engelbrecht, M. Randeria, and C. A. R. Sá de Melo, *Phys. Rev. B* **55**, 15153 (1997).
- [20] G. E. Astrakharchik, D. Blume, and S. Giorgini, unpublished (2006/2007).
- [21] K. Huang and C. N. Yang, *Phys. Rev.* **105**, 767 (1957).
- [22] D. Blume and C. H. Greene, *Phys. Rev. A* **65**, 043613 (2002).
- [23] E. L. Bolda, E. Tiesinga, and P. S. Julienne, *Phys. Rev. A* **66**, 013403 (2002).
- [24] T. Busch, B.-G. Englert, K. Rzazewski, and M. Wilkens, *Foundations of Phys.* **28**, 549 (1998).
- [25] E. Fermi, *Ric. Sci.* **7**, 13 (1936).
- [26] J. von Stecher and C. H. Greene, *Phys. Rev. A* **75**, 022716 (2007).
- [27] S. Y. Chang and G. F. Bertsch, *physics/0703190* (2007).
- [28] M. Brack and R. K. Bhaduri, *Semiclassical Physics* (Addison-Wesley, Reading, MA, 1997).
- [29] J. Carlson and S. Reddy, *Phys. Rev. Lett.* **95**, 060401 (2005).
- [30] T.-L. Ho, *Phys. Rev. Lett.* **92**, 090402 (2004).
- [31] S.-T. Wu, C.-H. Pao, and S.-K. Yip, *Phys. Rev. B* **74**, 224504 (2006).
- [32] J. Carlson, S. Y. Chang, V. R. Pandharipande, and K. E. Schmidt, *Phys. Rev. Lett.* **91**, 050401 (2003).
- [33] S. Y. Chang, V. R. Pandharipande, J. Carlson, and K. E. Schmidt, *Phys. Rev. A* **70**, 043602 (2004).
- [34] H. Caldas, C. W. Morais, and A. L. Mota, *Phys. Rev. D*

- 72**, 045008 (2005).
- [35] G.-D. Lin, W. Yi, and L.-M. Duan, Phys. Rev. A **74**, 031604 (2006).
- [36] M. Iskin and C. A. R. Sá de Melo, cond-mat/0604184 (2006).
- [37] M. Iskin and C. A. R. Sá de Melo, cond-mat/0606624 (2006).
- [38] M. M. Parish, F. M. Marchetti, A. Lamacraft, and B. D. Simons, Phys. Rev. Lett. **98**, 160402 (2007).
- [39] L. He, M. Jin, and P. Zhuang, Phys. Rev. B **73**, 220504(R) (2006).